

Understanding the Trade-offs in Accuracy and Uncertainty Quantification: Architecture and Inference Choices in Bayesian Neural Networks

Alisa Sheinkman* and Sara Wade*

June 18, 2025

Abstract

As modern neural networks get more complex, specifying a model with high predictive performance and sound uncertainty quantification becomes a more challenging task. Despite some promising theoretical results on the true posterior predictive distribution of Bayesian neural networks, the properties of even the most commonly used posterior approximations are often questioned. Computational burdens and intractable posteriors expose miscalibrated Bayesian neural networks to poor accuracy and unreliable uncertainty estimates. Approximate Bayesian inference aims to replace unknown and intractable posterior distributions with some simpler but feasible distributions. The dimensions of modern deep models, coupled with the lack of identifiability, make Markov chain Monte Carlo (MCMC) tremendously expensive and unable to fully explore the multimodal posterior. On the other hand, variational inference benefits from improved computational complexity but lacks the asymptotical guarantees of sampling-based inference and tends to concentrate around a single mode. The performance of both approaches heavily depends on architectural choices; this paper aims to shed some light on this, by considering the computational costs, accuracy and uncertainty quantification in different scenarios including large width and out-of-sample data. To improve posterior exploration, different model averaging and ensembling techniques are studied, along with their benefits on predictive performance. In our experiments, variational inference overall provided better uncertainty quantification than MCMC; further, stacking and ensembles of variational approximations provided comparable accuracy to MCMC at a much-reduced cost.

Keywords: Approximate Bayesian Inference, Bayesian Deep Learning, Ensembles, Out-of-Distribution, Uncertainty Quantification.

1 Introduction

Despite the tremendous success of deep learning in areas such as natural language processing [Touvron et al., 2023] and computer vision [Krizhevsky et al., 2017, Dosovitskiy et al., 2020], often there is no clear understanding of why a particular model performs well [Zhang et al., 2021, Szegedy et al., 2014]. Even though the universal approximation theorem guarantees that a wide enough feed-forward neural network with a single hidden layer can express any smooth function [Hornik et al., 1989], in practice, constructing a model which is not only

*School of Mathematics and Maxwell Institute for Mathematical Sciences, University of Edinburgh, a.sheinkman@sms.ed.ac.uk , sara.wade@ed.ac.uk

Table 1: Some of the challenges and properties of classical and Bayesian neural networks.

Property	Classical NN	Bayesian NN
Interpretability	poor	improved ✓
Robustness to OOD	poor	improved ✓
Adversarial attacks	sensitive	less sensitive ✓
Overconfidence	typical	less typical ✓
Training outcome	point estimate ·	posterior distribution \mathbb{P}
Incorporate prior	no	yes
Require initialization	yes	yes

expressive but generalizes well is challenging. In contrast, the so-called no free lunch theorem [Wolpert, 1996] dictates that there is no panacea to solve every problem, and one should be careful when designing a model appropriate to the task. Many modern machine learning models are over-parametrized and prone to overfitting, especially given the limited size of the dataset. Complex problems demand exploring bigger model spaces, and there is a danger of choosing an excessively over-parametrized model, which is going to overfit and have a high variance. Additionally, conventional deep models do not offer human-understandable explanations and lack interpretability [Lipton, 2018]. By default, classical neural networks do not address the uncertainty associated with their parameters and whilst there exist proposals enabling neural networks (NNs) to provide some uncertainty estimates, they are often miscalibrated [Guo et al., 2017]. As a result, these models are typically overconfident, provide a low level of uncertainty even when data variations occur [Ovadia et al., 2019], and are easily fooled and are susceptible to adversarial attacks [Szegedy et al., 2014, Nguyen et al., 2015]. At the same time, reliable uncertainty quantification (UQ) is crucial for any decision-making process, and it is not enough to obtain a point estimate of the prediction.

The key distinguishing property of the Bayesian framework is that it incorporates domain expertise and deals with uncertainty quantification in a principled way: by marginalizing with respect to the posterior distribution of parameters. As a result, Bayesian models are more resistant to distribution shifts and can improve the accuracy and calibration of classical deep models [Wilson and Izmailov, 2020]. Nevertheless, the reliability of uncertainty estimates and the gap between within-the-sample and out-of-sample performance still require improvement [Foong et al., 2020]. The posterior distributions arising in Bayesian neural networks (BNNs) are analytically unavailable and highly multimodal, and the core challenge lies in estimating the posterior [Papamarkou et al., 2022]. One should not only find a model that matches the task but, as importantly, achieve the alignment between the model and the applied inference algorithm [Gelman et al., 2020]; and the most theoretically grounded sampling methods and approximation techniques are limited by the computing budget, size of the dataset, and sheer number of parameters. We list several characteristics of classical and Bayesian neural networks in the Table 1.

Outline. In this work, we consider some of the challenges and nuances of Bayesian neural networks and evaluate the performance with different architectures and for different posterior inference algorithm choices. Specifically, we study the sensitivity of BNNs to the choice of width in Section 2.3, depth in Section 2.4, and investigate the performance of BNNs under the distribution shift in Section 2.5. Across all the experiments in Section 2, we observe that for different inference algorithms, one model can provide strikingly diverse performances. The challenge of comparative model assessment is addressed in Section 3.1,

where we introduce the estimated pointwise loglikelihood as a measure of model utility. While given some set of models, the Bayesian approach has the potential to deal with the model choice by comparing posterior model probabilities, such comparison tends to favour one candidate disproportionately strongly [Oelrich et al., 2020]. Thus, the classical Bayesian model averaging (BMA) based on model probabilities [Hoeting et al., 1999] is only optimal if the true model is among the comparison set. In response to the limitations of BMA, in Sections 3.2 to 3.4 we consider ensembling, stacking and pseudo-BMA[Yao et al., 2018].

2 Empirical Study of Limiting Scenarios

2.1 Architecture Components

Whilst the dimensions of the input and the output are determined by the dimensionality of the data set, the dimension of the weight space plays an essential part in specifying neural networks and can be tuned to improve prediction performance. In the case of feed-forward neural networks, this amounts to finding optimal depth and width. While the universal approximation theorem advocates for single-layer neural networks [Hornik et al., 1989], variants of the universal approximation theorem exist for deeper networks [Lu et al., 2017, Hanin, 2019]. Further, deep neural networks gained popularity due to their expressiveness and tremendous success in real-world applications, allowed by the increase in available computing power [Chatziafratis et al., 2020]. At the same time, the more parameters one has, the more nuanced the choice of the model becomes. No matter what the prediction task is, overly complex models suffer from the curse of dimensionality which causes not only poor performance but also computational problems.

On a slightly different line, we recall the seminal result first obtained for neural networks with one hidden layer [Neal, 1995] and then extended to arbitrary depth [Matthews et al., 2018] which states that under general conditions, as the width of a BNN tends to infinity, the distribution of the network’s output induced by the prior converges to a Gaussian process (GP) with a neural network kernel, also known as the neural network GP (NNGP); there is a similar correspondence relating GPs and distributions induced by the posterior [Hron et al., 2022]. When defining BNNs, choosing a prior and understanding how properties and prior beliefs on the weight space translate to the functions is a major challenge. Note that generally, we require priors which are: (1) interpretable, e.g. we want to be able to specify the hyperparameters of the prior based on the task at hand; (2) have large support, i.e. prior should not concentrate around a small subset of the parameter space; (3) lead to feasible inference and favour reasonable approximations of the posterior and predictive distributions.

Finally, to specify any neural network, one needs to choose the activation function, which (apart from being nonlinear) is required to be differentiable. In our experiments, we consider the widely-used rectified linear unit function (ReLU) defined as $\max(0, x)$, which switches the negative inputs off and leaves the positive ones unchanged, as well as the sigmoid activation function defined as $\sigma(x) = \exp(x)/(\exp(x) + 1)$.

2.2 Setup of the Experiments

In the experiments, we consider the following BNN, illustrated by the Figure 1a

$$\begin{aligned} \mathbf{y} &\sim \mathcal{N}(\mathbf{b}_{L+1} + \mathbf{W}_{L+1}\mathbf{z}_L, \boldsymbol{\sigma}), \quad \boldsymbol{\sigma} \sim |\mathcal{N}(0, 0.001)| \\ \mathbf{z}_l &= g(\mathbf{b}_l + \mathbf{W}_l\mathbf{z}_{l-1}) \text{ for } l = 1, \dots, L, \end{aligned} \tag{1}$$

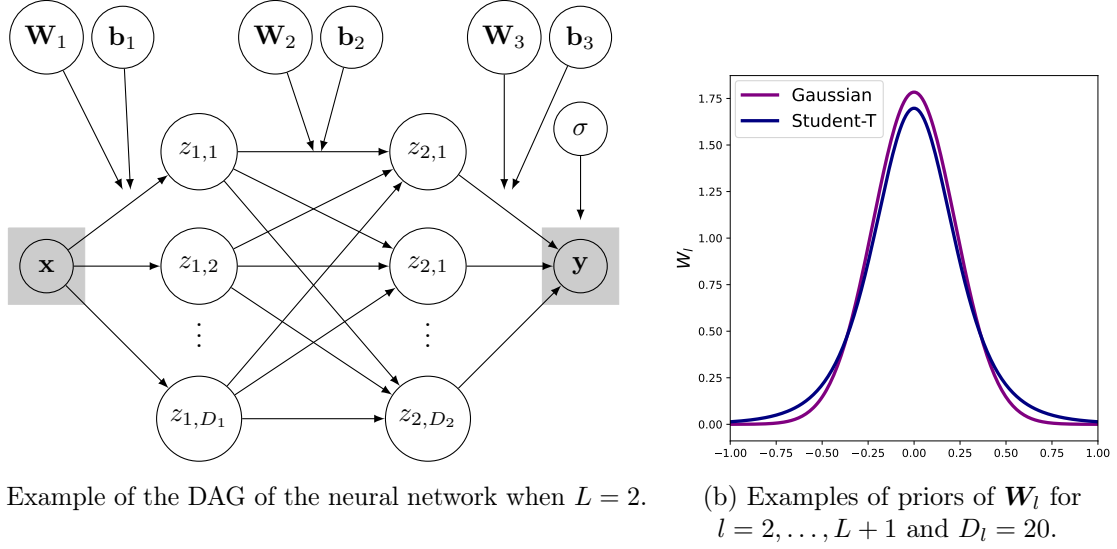


Figure 1: Examples of the directed acyclic graph (DAG) of the neural network and of the priors used in the experiments.

where we consider two different choices of activations g , namely, the ReLU and the sigmoid; $|\mathcal{N}(\cdot)|$ denotes a half-normal distribution; and $\mathbf{z}_0 = \mathbf{x}$. We consider two possible choices of priors on the weights (illustrated by Figure 1b): (i) Gaussian priors as the most conventional choice [Arbel et al., 2023, Fortuin, 2022]; (ii) Student-t priors, motivated by the observation that empirical weight distributions of SGD-trained networks are heavy-tailed [Fortuin et al., 2022, Gurbuzbalaban et al., 2021]. We finish specifying the model by placing Gaussian priors on the biases, that is:

$$\begin{aligned} \mathbf{W}_1 &\sim F\left(0, \frac{1}{4L}\right), \quad \mathbf{W}_l \sim F\left(0, \frac{4}{D_{l-1}}\right) \quad \text{for } l = 2, \dots, L + 1, \\ \mathbf{b}_l &\sim \mathcal{N}\left(0, \frac{1}{4L}\right) \quad \text{for } l = 1, \dots, L + 1, \end{aligned}$$

where the notation $F(\mu, \sigma^2)$ represents a distribution with mean μ and scale σ , and specifically, here is chosen as either Gaussian or Student-t with 5 degrees of freedom. To avoid divergence in wider networks and mitigate the damage caused by the nonlinear deformation [He et al., 2015], the weights' variance is scaled by the inverse of the preceding layer's width.

The BNN defined by Equation (1) and trained with automatic differentiation variational inference (ADVI) [Kucukelbir et al., 2017], which assumes a mean-field (diagonal) Gaussian variational family, is referred to as mfVIR or mfVIS, depending on the choice of the activation: ReLU or sigmoid, respectively. The model trained with the Hamiltonian Monte Carlo (HMC), using the No U-Turn Sampler (NUTS) [Hoffman and Gelman, 2014] is denoted as HMCR or HMCS. For simplicity, we often refer to one-layer neural networks of particular width D as to mfVIRD, mfVISD, HMCRD or HMCS (e.g. one-layer BNN with 20 hidden units and ReLU activation trained with mean-field VI is called mfVIR20). All experiments are implemented with Numpyro [Phan et al., 2019], ArviZ [Kumar et al., 2019], JAX [Bradbury et al., 2018] and Flax [Heek et al., 2024]. We record the run time of the approximate inference (TT), the root mean squared error RMSE and empirical coverage for the function and observations (EC). Note that we compute empirical coverage as a fraction of observations contained within

the 95% confidence interval (CI), this means that in the ideal settings the computed EC should equal to 0.95. If $EC > 0.95$ then the confidence intervals are too wide; a worse scenario occurs when $EC < 0.95$ as it means that the CIs are too narrow and the model is overconfident in predictions. Details on the computed metrics and the corresponding formulas are discussed in Appendix A, where we provide further information on the initialization and parameters for the inference algorithms¹.

The absence of the test log-likelihood among the recorded metrics is motivated by the observation that the higher test log-likelihood does not necessarily correspond to a more accurate posterior approximation nor to lower predictive error (such as RMSE)[Deshpande et al., 2024].

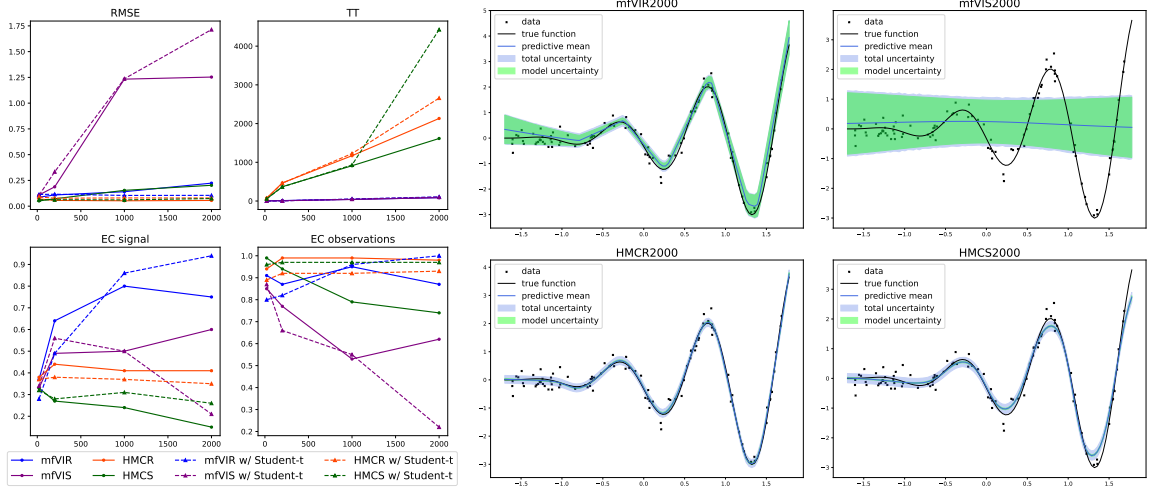
2.3 Increasing the Width of the Network

We consider a simple synthetic dataset with one-dimensional input and output:

$$\mathbf{x} \sim \text{Unif}([0, 2]), \mathbf{y} = \sin(10\mathbf{x})\mathbf{x}^2 + \epsilon, \epsilon \sim \text{N}(0, 0.25).$$

The training data \mathcal{D} consists of $N = 500$ observations and the new data for testing $\tilde{\mathcal{D}}$ consists of $\tilde{N} = 100$ observations. We first study the performances of mfVIR, mfVIS, HMCR and HMCS with 1 hidden layer and either Gaussian or Student-t priors as the width increases, and illustrate the metrics for $D_1 = 20, 200, 1000$ and 2000 hidden units by the Figure 2a. The predictions of the four combinations of activation and inference algorithm with Gaussian priors when $D_1 = 2000$ are provided on the Figure 2b; similar results were obtained when weights have Student-t distribution, the figures are presented in Appendix C. For either choice of priors, performance of the mfVIS dips with the increase in the dimension of the hidden layer; moreover, for $D_1 = 1000$ and $D_1 = 2000$ its posterior predictive distribution fails to capture the data, and, in fact, degenerates to the prior (Figure 2b). An explanation of why such behaviour occurs was obtained via the correspondence of Gaussian processes and BNNs. While as the width increases the true posterior of a BNN converges to a NNGP posterior [Hron et al., 2022], any optimal mean-field Gaussian variational posterior of a BNN with odd (up to a constant offset) Lipschitz activation function converges to the prior predictive distribution of the NNGP [Coker et al., 2022]. In other words, the mean-field variational approximations of wide BNNs with sigmoid activations ignore the data. If one abandons the mean-field assumption and proposes a full-rank variational family, then using variational inference (VI) for wider networks would take at least a hundred times more time than using HMC, which undermines the benefits of using VI. Such degenerate behaviour is not observed with HMC(Figure 2b, but this comes at a significant increase in training time. For wider networks, the HMCR model exhibits a better performance than the HMCS both in terms of accuracy and uncertainty quantification. In terms of predictive accuracy, HMC is preferred over mfVI in all of the combinations of the activation function and width. However, in terms of uncertainty quantification, the HMC is inferior to mfVI (with one exception of a BNN with Student-t priors, sigmoid activation and 2000 hidden units). In our experiment, HMC underestimates the uncertainty of the signal much more than VI (Figures 2a and 2b). Note that whilst variational inference is often cursed to underestimate the uncertainty[Trippe and Turner, 2018], that is not always the case [Blundell et al., 2015, Gal and Ghahramani, 2016]. Markov chain Monte Carlo (MCMC) methods are known to struggle to effectively

¹The code is available on GitHub.



(a) Metrics of methods as the number of hidden units increases. (b) Predictions and uncertainty estimates for each method with $D_1 = 2000$ and Gaussian priors.

Figure 2: Predictive performance of BNNs as the width increases.

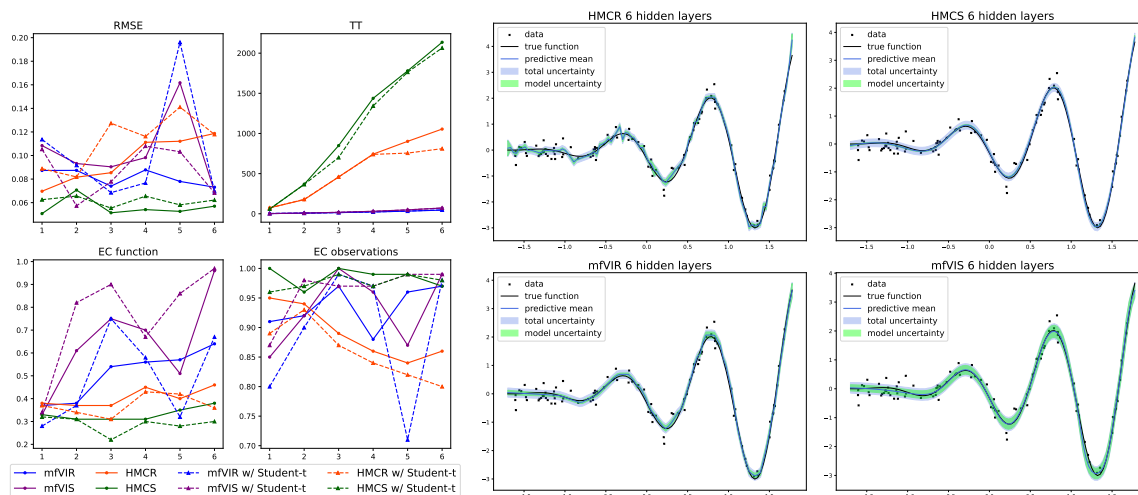
explore multimodal posteriors [Papamarkou et al., 2022, Izmailov et al., 2021], and a lack of uncertainty could be a result of poor mixing of the chain.

General summary. In wider networks, the ReLU is preferred over the sigmoid activation for both HMC and mfVI. Crucially, **when it comes to the mean-field VI the sigmoid activation should only be used when the limited width is suitable for the task at hand.** It is reasonable to suppose that the same could be said about any odd (up to adding a constant) activation function. Further, while the HMC was preferred over the mfVI when looking at accuracy alone, the required computational resources could be an obstacle. Moreover, uncertainty quantification is far from ideal for HMC (CIs are too narrow for the signal); instead, mfVI with the ReLU achieves a good balance between accuracy, UQ, and time, particularly for wider networks.

2.4 Increasing the Depth of the Networks

Consider the data of Section 2.3 and neural networks defined by Equation (1) with the number of layers L varying from 1 to 6 and a fixed number of hidden units in each layer $D_h = 20$. Figure 3a provides the recorded metrics, and Figure 3b illustrates the predictions of the four combinations of activation and inference algorithm with $L = 6$ and Gaussian priors (analogous figures for Student-t priors are provided in Appendix C). First, observe that overall both RMSE and empirical coverage of mfVIR approximations improve with the increase of depth, with one exception of $L = 5$ and Student-t priors, when the prediction quality of the network drops drastically. The mfVIS follows a similar pattern, except for the case of $L = 5$ and Gaussian priors. Indeed, the approximate posteriors of deep neural networks obtained with the mean-field variational inference were shown to be as flexible as the much richer approximate posteriors of shallower BNNs [Farquhar et al., 2020]. We do not obtain the same improvement in the prediction quality of models trained with HMC: for either choice of priors, the performance of HMCR falls, whilst the HMCS does not improve as the depth increases. This undesirable behaviour could be a result of the multimodality of distributions in overparametrized models combined with the challenges of MCMC in exploring

the high-dimensional space [Izmailov et al., 2021, Papamarkou et al., 2022]. Compared to the findings of Section 2.3, we note that the deeper NNs are less sensitive to the choice of the activation function. It is needless to say that the HMC algorithm scales rather poorly, and as the number of layers changes from $L = 1$ to $L = 6$, the time needed to train HMCR and HMCS gets more than 15 and 30 times greater, respectively. We note that for models with more than one hidden layer, training of the network with sigmoid activations takes roughly twice as much time as the network with ReLU. The striking discrepancy in training times could arise due to the difference in the leapfrog integrator step sizes [Betancourt et al., 2015].



(a) Metrics of methods as the number of hidden layers increases. (b) Predictions and uncertainty estimates for each method when $L = 6$ and Gaussian priors.

Figure 3: Prediction performance of BNNs as the depth increases.

General summary. In terms of the training time, HMC becomes less and less feasible with the increase in depth. With the need to explore high-dimensional parameter spaces, multimodality of the posteriors should be kept in mind as an arising challenge for both mFVI and HMC. **In terms of the balance between accuracy and UQ, the mean-field variational inference with ReLU activation function is able to outperform MCMC with the increase in depth.**

2.5 Out-of-Distribution Prediction

While it is not surprising that the accuracy and the quality of uncertainty quantification of any model decreases under a distribution shift, reliable uncertainty estimates that are robust to the out-of-distribution (OOD) data become exceptionally important in safety-critical applications. The challenge is especially intricate since better accuracy and lower calibration error of a certain model on the in-domain data do not imply better accuracy and lower calibration error in the OOD settings [Ovadia et al., 2019]. Here, we wish to validate the models' predictive abilities when the test data points come from previously unseen regions of data space. The kind of out-of-distribution data we consider could be described as 'complement-distributions', such data arises in open-set recognition or could be the result of an adversary [Farquhar and Gal, 2022]. Note that in Section 3.3 as well as in the supplementary, we consider a much milder example with 'related-distributions' data.

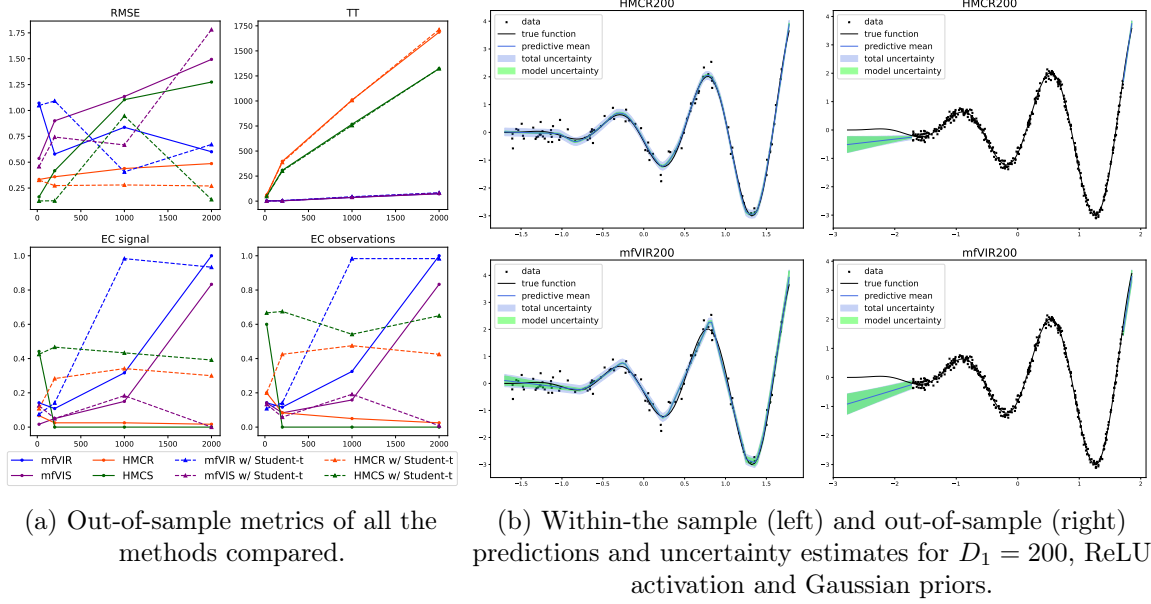


Figure 4: Out-of-distribution prediction for the 'complement-distributions' data.

We split the training data used in Sections 2.3 and 2.4 into the train and test data covering complement regions of the function.

Specifically, $\mathcal{D} = \mathcal{D}_c \sqcup \tilde{\mathcal{D}}_c$, the observed data \mathcal{D}_c consists of $N = 370$, the new data $\tilde{\mathcal{D}}_c$ consists of $\tilde{N} = 130$ and the observed and the new data are disjoint (see Figure 4):

$$\begin{aligned}\mathcal{D}_c &= \{(x_n, y_n) \mid x_n \in [-1.7, 1.7]\}, \\ \tilde{\mathcal{D}}_c &= \{(x_n, y_n) \mid x_n \in [-2.8, -1.7) \cup (1.7, 1.9]\}.\end{aligned}$$

Strictly speaking, we do not expect any model to be robust to such an extreme case and, mainly, want to assess and better understand the quality of the uncertainty estimates. In this experiment, we are hoping that the relationship between the distributions of the observed and the new data makes this challenge somewhat tractable. On Figure 4a we illustrate the metrics for $D_1 = 20, 200, 1000$ and 2000 hidden units; Figure 4b compares non-OOD and OOD predictions obtained by the BNNs with ReLU activation, Gaussian priors and $D_1 = 200$. The poor performance of the mfVIS, especially for wider networks, is not surprising, however, we notice that for wide networks HMCS with Gaussian priors suffers from much higher RMSE than HMCS with Student-t priors and mfVIR and HMCR with either choice of priors. And while HMCR has a lower RMSE than any model trained with mean-field VI, the ability of HMC to capture the uncertainty deteriorates, and it becomes overconfident. Whilst HMCR200 and mfVIR200 do not show any of the expected increase in the uncertainty, on certain regions both methods are able to provide accurate predictive mean (see Figure 4b for examples with Gaussian priors, the right-hand side region of the function, where $x > 1.5$). Finally, as the width of the network increases, mfVIR outperforms all of the methods.

General summary. In terms of the accuracy alone, the HMC with ReLU is more robust to the out-of-distribution data, however, that comes with the largest computational costs among all the models. We already saw in Section 2.3 that uncertainty quantification with HMC degrades with increasing width. In OOD settings, this becomes even more extreme, with very overconfident predictions that do not cover the truth (an empirical coverage of

almost zero). **Finally, with the increase in depth, in the extreme OOD settings, the mfVI with ReLU becomes almost as accurate as HMC with ReLU and provides better UQ at a much lower cost.**

3 Bayesian Model Averaging and Stacking

3.1 Predictive Methods for Model Assessment

When considering synthetic datasets, we can choose a desired metric and sample any number of data points, so that evaluation of the model’s performance becomes trivial. For example, in Section 2.5 we have specifically created an extreme case when the training data \mathcal{D}_c and the new data $\tilde{\mathcal{D}}_c$ were covering disjoint regions of the true function. In reality, the new previously unseen data is not available, and one can only estimate the expected out-of-sample predictive performance. Suppose that we only observe \mathcal{D} , the unseen observations $\tilde{\mathcal{D}}$ are generated by $p_t(\tilde{\mathcal{D}})$, and we wish to be able to assess the generalization ability of the model without having access to the test data. To keep the notation simple, we omit the dependency on \mathbf{x} and $\tilde{\mathbf{x}}$ when writing down the posteriors in this section. Given a new data point \tilde{y}_n , the log score $\log p(\tilde{y}_n|\mathcal{D})$ is one of the most common utility functions used in measuring the quality of the predictive distribution. The log score benefits from being a local and proper scoring rule [Vehtari and Ojanen, 2012]. Then, the expected log pointwise predictive density for a new dataset serves as a measure of the predictive accuracy of a given model:

$$\text{elpd} = \sum_{n=1}^{\tilde{N}} \int p_t(\tilde{\mathcal{D}}_n) \log p(\tilde{y}_n|\mathcal{D}) d\tilde{\mathcal{D}}_n,$$

where $p(\tilde{y}_n|\mathcal{D})$ is model’s posterior predictive distribution. In the absence of $\tilde{\mathcal{D}}$, one might obtain an estimate of the expected log pointwise predictive density by re-using the observed \mathcal{D} . Here, we review the approach that employs leave-one-out cross-validation (LOO-CV), which can be seen as a natural framework for assessing the model’s predictive performance [Vehtari et al., 2016].

To obtain the Bayesian leave-one-out cross-validation (LOO-CV) estimate of the expected utility $\widehat{\text{elpd}}_{\text{loo}}$ and avoid re-fitting the model N times, one could use importance sampling. However, the classical importance weights would have a large variance, and the obtained estimates would be noisy. Recently, the problem was solved with Pareto smoothed importance sampling (PSIS), which allows evaluating the LOO-CV expected utility in a reliable yet efficient way [Vehtari et al., 2016]:

$$\widehat{\text{elpd}}_{\text{loo}} = \sum_{n=1}^N p(y_n|x_n, \mathcal{D}_{-n}) = \sum_n \log \left(\frac{\sum_{s=1}^S r_i^s p(y_n|\theta^s)}{\sum_{s=1}^S r_i^s} \right), \quad (2)$$

where r_i^s are the smoothed importance weights, which benefit from smaller variance than the classical weights. We refer to the individual logarithms in the sum as $\widehat{\text{elpd}}_{\text{loo},n}$. The advantage of PSIS is that the estimated shape parameter of the Pareto distribution provides a diagnostic of the reliability of the resulting expected utility. Although methods of model selection which reuse the data can be vulnerable to overfitting when the size of the dataset is too small and/or the data is sparse, it is (relatively) safe to use cross-validation to compare a small number of models and given a large enough dataset [Vetari et al., 2019]. In Appendix B, we implement $\widehat{\text{elpd}}_{\text{loo}}$ in the empirical experiment, where we additionally consider posterior

predictive checks (PPC) and an alternative to the LOO-CV approach of estimating the expected log pointwise utility.

3.2 Alternatives to Classical Bayesian Model Averaging

Let $\mathcal{M} = \{M_1, \dots, M_K\}$ be a collection of models and denote the parameters of each of the M_k as θ_k . The assumptions one has on the prediction task and on \mathcal{M} with respect to the true data-generating process can be categorized into three scenarios: \mathcal{M} -closed, \mathcal{M} -open and \mathcal{M} -complete. If $M_k \in \mathcal{M}$ for some k recovers the true data generating process, then we are in the \mathcal{M} -closed case. The task is \mathcal{M} -complete if there exists a true model but it is not included in \mathcal{M} (e.g. for computational reasons). Finally, we are in the \mathcal{M} -open scenario when the true model is not in \mathcal{M} and the data-generating mechanism cannot be conceptually formalized to provide an explicit model [Vehtari and Ojanen, 2012]. The Bayesian framework allows to define the probabilities over the model space, and for the \mathcal{M} -closed case, classical Bayesian Model Averaging (BMA) would give optimal performance. The BMA solution provides an averaged predictive posterior as [Hoeting et al., 1999]

$$p(\tilde{\mathbf{y}} \mid \mathcal{D}) = \sum_{k=1}^K p(\tilde{\mathbf{y}} \mid \mathcal{D}, M_k) p(M_k \mid \mathcal{D}), \quad (3)$$

$$\text{where } p(M_k \mid \mathcal{D}) \propto p(\mathcal{D} \mid M_k) p(M_k). \quad (4)$$

However, in the \mathcal{M} -open and \mathcal{M} -complete prediction tasks, BMA is not appropriate as it gives a strong preference to a single model and so assumes that this particular model is the true one. Now, if we replace the weights $p(M_k \mid \mathcal{D})$ with the products of Bayesian LOO-CV densities $\prod_{n=1}^N p(y_n \mid x_n, \mathcal{D}_{-n}, M_k)$, we arrive at pseudo-Bayesian model averaging (pseudo-BMA). In other words, the weights w_k of pseudo-BMA are proportional to the estimated log pointwise predictive density $\exp(\widehat{\text{elpd}}_{\text{loo}}^k)$ introduced in Section 3.1. One could further correct each $\widehat{\text{elpd}}_{\text{loo}}$ estimate of Equation (2) by the standard errors and obtain

$$w_k = \frac{\exp(\widehat{\text{elpd}}_{\text{loo}}^{k,\text{reg}})}{\sum_{k=1}^K \exp(\widehat{\text{elpd}}_{\text{loo}}^{k,\text{reg}})},$$

$$\widehat{\text{elpd}}_{\text{loo}}^{k,\text{reg}} = \widehat{\text{elpd}}_{\text{loo}}^k - \frac{1}{2} \sqrt{\sum_{n=1}^N \left(\widehat{\text{elpd}}_{\text{loo},n}^k - \frac{\widehat{\text{elpd}}_{\text{loo}}^k}{N} \right)^2},$$

where for each model M_k we find $\widehat{\text{elpd}}_{\text{loo}}^{k,\text{reg}}$ by utilizing a log-normal approximation. Fortunately, we have already seen that these densities can be efficiently estimated with PSIS.

An alternative way to obtain the averaged predictive posterior given the set of $p(\tilde{\mathbf{y}} \mid \mathcal{D}, M_k)$ is to employ the stacking approach [Yao et al., 2018]. Define the set $S^K = \{\mathbf{w} \in [0, 1]^K \mid \sum_k^K w_k = 1\}$, then the stacking weights are found as the optimal (according to the logarithmic score) solution of the following problem

$$\begin{aligned} \mathbf{w} &= \max_{\mathbf{w} \in S^K} \frac{1}{N} \sum_{n=1}^N \log \sum_{k=1}^K w_k p(y_n \mid \mathcal{D}_{-n}, M_k), \\ &= \max_{\mathbf{w} \in S^K} \frac{1}{N} \sum_{n=1}^N \log \sum_{k=1}^K w_k \left(\frac{\sum_{s=1}^S r_i^s p(y_n \mid \theta_k^s, M_k)}{\sum_{s=1}^S r_i^s} \right), \end{aligned}$$

where a PSIS estimate of the predictive LOO-CV density is used, and r_i^s are the smoothed (truncated) importance weights.

Finally, we recall that deep ensembles of classical non-Bayesian NNs [Lakshminarayanan et al., 2017] behave similarly to Bayesian model averages, and both lead to solutions strongly favouring one single model [Wilson and Izmailov, 2020]. In contrast, the ensembles of BNN posteriors in Equation (3) with $p(M_k | \mathcal{D}) = K^{-1}$ can be seen as a trivial case of BMA, which combines models and does not give preference to a single solution. Alternatively, when implementing variational inference and combining BNNs, the analogy can be drawn with the simplified version of adaptive variational Bayes, which combines variational posteriors with certain weights and, under certain conditions, attains optimal contraction rates [Ohn and Lin, 2024].

3.3 Ensembles and Averages

We compare three model averaging methodologies: deep ensembles of Bayesian neural networks, stacking and pseudo-BMA based on PSIS-LOO [Yao et al., 2018]. We do not consider the Bayesian Bootstrap (BB) [Rubin, 1981] motivated by the recent observation that in the settings of modern neural networks deep ensembles of non-Bayesian NNs and BB are equivalent, and both are often misspecified [Wu and A Williamson, 2024]. Combining several estimates of BNNs can be effective not only when predictions are coming from different models, but also when dealing with several predictions obtained by the same model [Ohn and Lin, 2024]. This is of particular use for multimodal posteriors arising in BNNs, where different modes could be explored by random initializations [Yao et al., 2018]. Additionally, recall that the ELBO, the objective of variational inference, is a non-convex function, so that the optimum is only local and depends on the starting point. We note that combining models trained with HMC and VI would be meaningless for several reasons. First of all, training a set of HMC models becomes rather expensive: for instance, training the HMC20 once takes the same amount of time as 35 trainings of mfVIR20. Second, the estimates of the log pointwise predictive densities (provided in Appendix B) for HMC and VI have different scales and are not easily compared; in this case, the result of averaging HMC and VI would be equivalent to classical BMA.

Now consider the mfVIR20 model with Gaussian priors and the 'complement-distributions' data of Section 2.5. We choose 10 random initialization points, obtain 10 posterior predictive distributions and compute estimated expected log pointwise predictive densities. We then construct ensemble, pseudo-BMA and stacking approximations; the results are illustrated Figure 5. Ensembling and stacking are superior to pseudo-BMA, which has worse accuracy and fails to capture any uncertainty. Similar results for the mfVIR20 model with Student-t priors are provided in Appendix C.

Given the nature of the test data we use, the predictions as well as the $\widehat{\text{elpd}}_{\text{loo}}$ estimates may be unreliable. Thus, we consider a simpler data-generating mechanism in which test data comes from a slightly broader region; such a scenario could be called an OOD task with 'related-distributions' [Farquhar and Gal, 2022]. Specifically, the data are generated as follows:

$$\mathbf{x} \sim \text{Unif}([0, 1]), \quad \mathbf{y} = \sin(10\mathbf{x})\mathbf{x}^2 + \boldsymbol{\epsilon}, \quad \boldsymbol{\epsilon} \sim 0.05\text{N}(\mathbf{0}, \mathbf{I}).$$

The data for training \mathcal{D}_r and the testing $\tilde{\mathcal{D}}_r$ consist of $N = 450$ and $\tilde{N} = 50$ observations, respectively, where $\tilde{\mathcal{D}}_r$ comes from the broader region than \mathcal{D}_r , i.e. $(\min_{n=1\dots N}(x_n), \max_{n=1\dots N}(x_n)) \subsetneq (\min_{n=1\dots \tilde{N}}(\tilde{x}_n), \max_{n=1\dots \tilde{N}}(\tilde{x}_n))$. For 10 posterior predictive distributions of mfVIR20 with

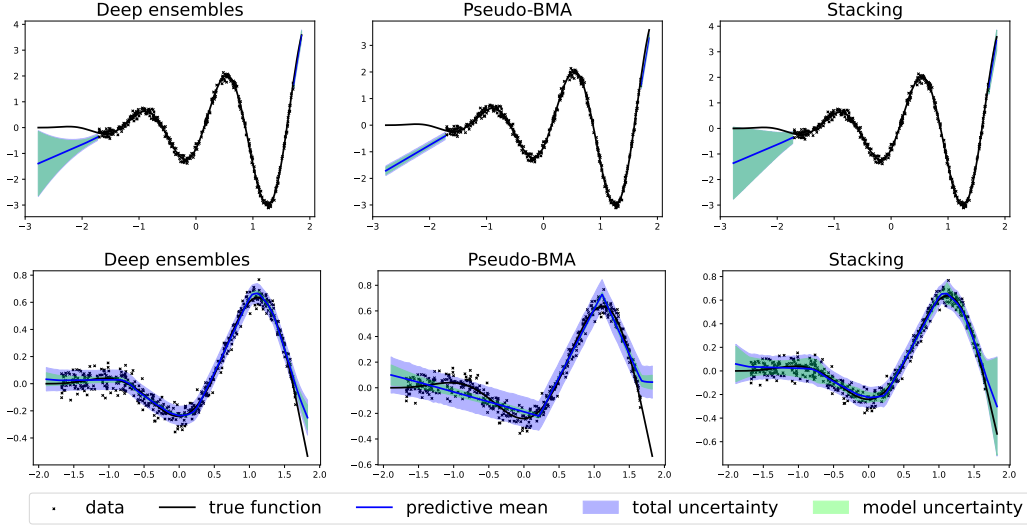


Figure 5: Predictions obtained by ensembling, stacking and pseudo-BMA when applied to mfVIR20 with Gaussian priors in the ‘complement-distributions’ (top) and ‘related-distributions’ (bottom) OOD tasks. Pseudo-BMA is worse than the other methodologies, and stacking provides improvements over DE in uncertainty quantification.

Gaussian priors (results for Student-t priors are provided in Appendix C), we compare ensembling, pseudo-BMA and stacking in Figure 5 (similar results with having Student-t priors are presented in the supplementary, and in Appendix D.2 we additionally provide the results of ensembling and averaging in the deeper networks.). Whilst the total uncertainty estimates of pseudo-BMA are, somewhat, adequate, the model uncertainty is underestimated. Both stacking and deep ensembles lead to improved predictive performance and uncertainty quantification, with stacking showing some better gains compared to deep ensembles (see e.g. improved coverage of stacking on the right-hand side of Figure 5).

General summary. We observe that, similar to BMA, the pseudo-BMA is not preferable in \mathcal{M} -open and \mathcal{M} -complete settings. Namely, in ‘complement-distributions’ and ‘related-distributions’ experiments, pseudo-BMA was confirmed to be inferior to stacking and ensembles of BNNs both in terms of the predictive accuracy and uncertainty quantification. Stacking and ensembles of BNNs performed comparable to each other and provided an improvement, with modest gains for stacking, which is especially significant in terms of uncertainty quantification in the OOD setting.

3.4 The Rocket Booster Simulation

We further evaluate the empirical performance of Bayesian model averaging techniques in BNNs by considering the data simulated by NASA when designing a novel rocket booster called Langley Glide-Back Booster (LGBB) [Gramacy and Lee, 2008, Rogers et al., 2003]. The data comprises 3167 observations, and the goal is to model the lift force as a function of the speed of the vehicle, the angle of attack α , and the sideslip angle β . Speed ranges from Mach 0 to Mach 6, the angle α lies in between -5 and 30 degrees and the sideslip angle β takes values $0, 0.5, 1, 2, 3, 4$.

We begin with the non-OOD scenario, consider a one-layer BNN with ReLU activation,

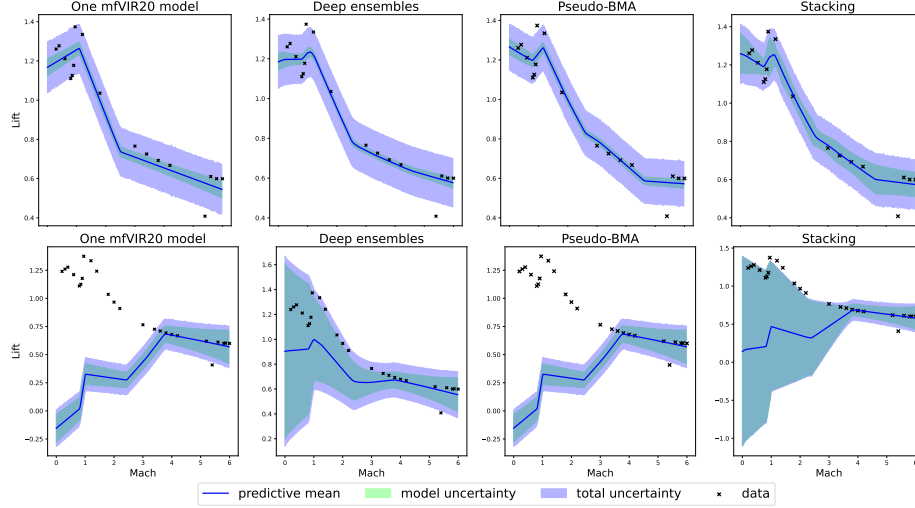


Figure 6: Slices of predicted lift obtained by a single model and by ensembling, stacking and pseudo-BMA when applied to mfVIR20 with Gaussian priors in the non-OOD (top) and 'complement-distributions' OOD (bottom) tasks.

Gaussian prior and $D_1 = 20, 100$ or 200 and train our model with mfVI on 80% of the data. Figure 6 displays a slice of predicting lift, with Mach (speed) on the x-axis, α fixed to 25 and β to 4; it compares predictions of a single mfVIR20 model to the results of combining 10 predictive distributions via deep ensembles, pseudo-BMA and stacking. Figures for slices of predicting lift obtained for models with 100 and 200 hidden units are provided in Appendix D.3. Figure 7 compares the metrics obtained by different approaches as the BNN gets wider. Stacking provides modest gains in accuracy, and while coverage is comparable across all methods, the slightly wider model uncertainty visible in the top row Figure 6 for stacking seems more reasonable given the observed data (crosses).

Further, we construct the 'complement-distributions' OOD scenario: the data taken for training consists of all datapoints but those whose sideslip angle β equals 4, the data on which we then test the model consists of the remaining datapoints for which $\beta = 4$. Similar to the non-OOD scenario, Figure 6 (bottom) compares slices of predicting lift obtained by a single mfVIR20 model to the predictions of deep ensembles, pseudo-BMA and stacking (figures for models with 100 and 200 hidden units are provided in Appendix D.3); this figure particularly highlights how a single model and pseudo-BMA can lead to incorrect, overconfident predictions in OOD settings. Unlike the non-OOD case, where performance is stable across the network's width, it varies substantially for OOD (left versus right side of Figure 6), especially for pseudo-BMA and stacking, which show improvements in both accuracy and uncertainty as the width increases.

General summary. In the non-OOD scenario, stacking provides modest gains in both accuracy and uncertainty quantification, compared to deep ensembles and pseudo-BMA, with stable performance across different widths. **Instead, for the 'complement-distributions' OOD task, performance heavily depends on the network architecture. Deep ensembles show the most stability, with stacking and pseudo-BMA becoming competitive as the width increases.**

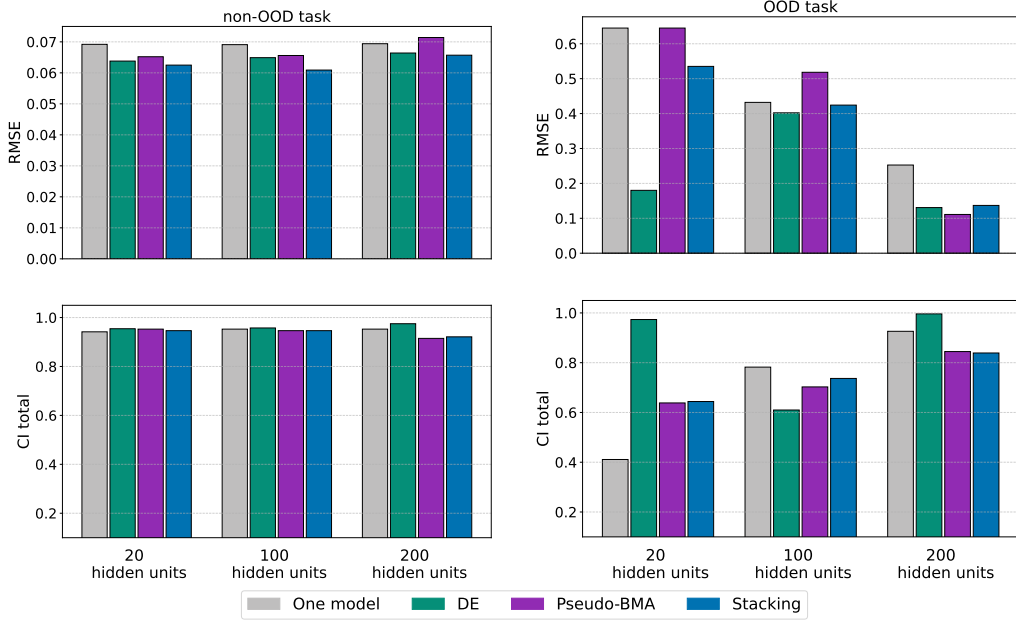


Figure 7: RMSE and CI obtained by a single mfVIR model, and by ensembling, stacking and pseudo-BMA when applied to mfVIR20 with Gaussian priors in the non-OOD (LHS) and 'complement-distributions' OOD (RHS) tasks.

4 Discussion

The message of an optimist's conclusion could question the common belief that the mean-field variational approximations are generally overly restrictive and do not capture the true posterior and the uncertainty well. Even with increases in computing power, the computational costs of sampling algorithms suggest that it may not be feasible for most modern neural networks and datasets. Moreover, although HMC is often considered as a gold standard, we have seen this may not be the case for BNNs due to complexity and multimodality of the posterior. Indeed, in a variety of experiments considered in Sections 2.3 to 2.5 and 3.3 **mfVI overall provided better uncertainty quantification than HMC**, and in out-of-distribution settings, the empirical coverage of the latter was close to zero. We note that **for single-layer neural networks, HMC outperformed mfVI only in terms of accuracy**. At the same time, for deeper networks and in out-of-distribution scenarios, the accuracy of mfVI was often comparable to HMC. Further, in Section 2.4 we confirmed that even for slightly deeper networks the time needed for HMC becomes a burden, which makes variational inference a very attractive alternative to sampling. Nevertheless, in Section 2.3 we observed that **the restrictions imposed by the factorized families can obstruct models from effectively learning from the data**. In real-life scenarios where one is required to evaluate the future predictive performance of the model before applying it to the unseen data, the estimate of the expected log pointwise predictive density can serve as a reliable diagnostic and thus, PSIS-LOO estimates can be beneficial for model assessment and combination. In Sections 3.3 and 3.4, **stacking and ensembles of BNNs were shown to be a possible solution when dealing with multimodal posteriors, helping to both improve accuracy and uncertainty quantification even in the extreme OOD scenario**. We find that stacked or ensembled variational approximations are competitive to

HMC at a much-reduced cost. Not only do the performance of individual models depend on architectural choices, but as observed in Section 3.4, the model averaging techniques are themselves influenced by these modelling choices. Finally, we note that overall in our experiments, there was no considerable and systematic difference in the performance between the BNNs with Gaussian and Student-t priors.

This work highlights the model’s sensitivity to architectural choices, namely, width, depth and activation function. Future work could study the performance of various more elaborate than Gaussian or Student-t choices of priors placed on the weights, including sparsity-inducing priors which have been shown to improve the accuracy and calibration [Blundell et al., 2015, Polson and Ročková, 2018]. Further, an important avenue for research is to consider the so-called structured variational inference with less restrictive variational families, and more generally, study the trade-off between the expressiveness of the variational family and scalability. Finally, given the multimodal nature of distributions arising in Bayesian neural networks, a promising avenue for research is to continue improving model combination techniques. This includes developing a better understanding of the number of models required for optimal performance with existing ensembling methods, as well as exploring more advanced approaches such as adaptive variational Bayes frameworks [Ohn and Lin, 2024] or hierarchical stacking and pointwise model combination [Yao et al., 2022].

References

- Hiroto Akaike. *Information Theory and an Extension of the Maximum Likelihood Principle*, pages 199–213. Springer New York, New York, NY, 1998. ISBN 978-1-4612-1694-0. doi: 10.1007/978-1-4612-1694-0_15.
- Julyan Arbel, Konstantinos Pitas, Mariia Vladimirova, and Vincent Fortuin. A primer on bayesian neural networks: review and debates. *arXiv preprint arXiv:2309.16314*, 2023.
- M. J. Betancourt, Simon Byrne, and Mark Girolami. Optimizing the integrator step size for hamiltonian monte carlo, 2015.
- Charles Blundell, Julien Cornebise, Koray Kavukcuoglu, and Daan Wierstra. Weight uncertainty in neural network. In *Proceedings of The International conference on machine learning*, pages 1613–1622. PMLR, 2015.
- James Bradbury, Roy Frostig, Peter Hawkins, Matthew James Johnson, Chris Leary, Dougal Maclaurin, George Necula, Adam Paszke, Jake VanderPlas, Skye Wanderman-Milne, and Qiao Zhang. Jax: composable transformations of python+numpy programs, 2018. URL <http://github.com/jax-ml/jax>.
- Vaggos Chatziafratis, Sai Ganesh Nagarajan, and Ioannis Panageas. Better depth-width trade-offs for neural networks through the lens of dynamical systems. In *Proceedings of The International Conference on Machine Learning*, pages 1469–1478. PMLR, 2020.
- Beau Coker, Wessel P Bruinsma, David R Burt, Weiwei Pan, and Finale Doshi-Velez. Wide mean-field bayesian neural networks ignore the data. In *International Conference on Artificial Intelligence and Statistics*, pages 5276–5333. PMLR, 2022.
- Sameer K Deshpande, Soumya Ghosh, Tin D Nguyen, and Tamara Broderick. Are you using test log-likelihood correctly? *Transactions on machine learning research*, 2024.

- Alexey Dosovitskiy, Lucas Beyer, Alexander Kolesnikov, Dirk Weissenborn, Xiaohua Zhai, Thomas Unterthiner, Mostafa Dehghani, Matthias Minderer, Georg Heigold, Sylvain Gelly, et al. An image is worth 16x16 words: Transformers for image recognition at scale. In *International Conference on Learning Representations*, 2020.
- Sebastian Farquhar and Yarin Gal. What ‘out-of-distribution’ is and is not. In *NeurIPS ML Safety Workshop*, 2022.
- Sebastian Farquhar, Lewis Smith, and Yarin Gal. Liberty or depth: Deep bayesian neural nets do not need complex weight posterior approximations. *Advances in Neural Information Processing Systems*, 33:4346–4357, 2020.
- Andrew Foong, David Burt, Yingzhen Li, and Richard Turner. On the expressiveness of approximate inference in bayesian neural networks. *Advances in Neural Information Processing Systems*, 33:15897–15908, 2020.
- Vincent Fortuin. Priors in bayesian deep learning: A review. *International Statistical Review*, 90(3):563–591, 2022.
- Vincent Fortuin, Adrià Garriga-Alonso, Sebastian W. Ober, Florian Wenzel, Gunnar Rätsch, Richard E. Turner, Mark van der Wilk, and Laurence Aitchison. Bayesian neural network priors revisited, 2022.
- Yarin Gal and Zoubin Ghahramani. Dropout as a bayesian approximation: Representing model uncertainty in deep learning. In *international conference on machine learning*, pages 1050–1059. PMLR, 2016.
- Andrew Gelman, Jessica Hwang, and Aki Vehtari. Understanding predictive information criteria for bayesian models. *Statistics and computing*, 24:997–1016, 2014.
- Andrew Gelman, Aki Vehtari, Daniel Simpson, Charles C. Margossian, Bob Carpenter, Yuling Yao, Lauren Kennedy, Jonah Gabry, Paul-Christian Bürkner, and Martin Modrák. Bayesian workflow, 2020.
- Robert B Gramacy and Herbert K H Lee. Bayesian treed gaussian process models with an application to computer modeling. *Journal of the American Statistical Association*, 103(483):1119–1130, 2008.
- Chuan Guo, Geoff Pleiss, Yu Sun, and Kilian Q. Weinberger. On calibration of modern neural networks. In *Proceedings of The International Conference on Machine Learning*, volume 70 of *Proceedings of Machine Learning Research*, pages 1321–1330. PMLR, 06–11 Aug 2017.
- Mert Gurbuzbalaban, Umut Simsekli, and Lingjiong Zhu. The heavy-tail phenomenon in sgd. In *Proceedings of the 38th International Conference on Machine Learning*, volume 139 of *Proceedings of Machine Learning Research*, pages 3964–3975. PMLR, 18–24 Jul 2021.
- Boris Hanin. Universal function approximation by deep neural nets with bounded width and relu activations. *Mathematics*, 7(10):992, 2019.
- Kaiming He, Xiangyu Zhang, Shaoqing Ren, and Jian Sun. Delving deep into rectifiers: Surpassing human-level performance on imagenet classification. In *Proceedings of the IEEE international conference on computer vision*, pages 1026–1034, 2015.

- Jonathan Heek, Anselm Levskaya, Avital Oliver, Marvin Ritter, Bertrand Rondepierre, Andreas Steiner, and Marc van Zee. Flax: A neural network library and ecosystem for JAX, 2024. URL <http://github.com/google/flax>.
- Jennifer A Hoeting, David Madigan, Adrian E Raftery, and Chris T Volinsky. Bayesian model averaging: A tutorial. *Statistical Science*, 14(4):382–417, 1999.
- Matthew D. Hoffman and Andrew Gelman. The no-u-turn sampler: Adaptively setting path lengths in hamiltonian monte carlo. *Journal of Machine Learning Research*, 15(47):1593–1623, 2014.
- Kurt Hornik, Maxwell Stinchcombe, and Halbert White. Multilayer feedforward networks are universal approximators. *Neural Networks*, 2(5):359–366, 1989. ISSN 0893-6080.
- Jiri Hron, Roman Novak, Jeffrey Pennington, and Jascha Sohl-Dickstein. Wide bayesian neural networks have a simple weight posterior: theory and accelerated sampling. In *Proceedings of the 39th International Conference on Machine Learning*, volume 162 of *Proceedings of Machine Learning Research*, pages 8926–8945. PMLR, 17–23 Jul 2022.
- Pavel Izmailov, Sharad Vikram, Matthew D Hoffman, and Andrew Gordon Gordon Wilson. What are bayesian neural network posteriors really like? In *Proceedings of the 38th International Conference on Machine Learning*, volume 139 of *Proceedings of Machine Learning Research*, pages 4629–4640. PMLR, 18–24 Jul 2021.
- Alex Krizhevsky, Ilya Sutskever, and Geoffrey E. Hinton. Imagenet classification with deep convolutional neural networks. *Commun. ACM*, 60(6):84–90, May 2017. ISSN 0001-0782.
- Alp Kucukelbir, Dustin Tran, Rajesh Ranganath, Andrew Gelman, and David M Blei. Automatic differentiation variational inference. *Journal of machine learning research*, 18(14):1–45, 2017.
- Ravin Kumar, Colin Carroll, Ari Hartikainen, and Osvaldo Martin. Arviz a unified library for exploratory analysis of bayesian models in python. *Journal of Open Source Software*, 4(33):1143, 2019.
- Balaji Lakshminarayanan, Alexander Pritzel, and Charles Blundell. Simple and scalable predictive uncertainty estimation using deep ensembles. In *Advances in Neural Information Processing Systems*, volume 30. Curran Associates, Inc., 2017.
- Zachary C Lipton. The mythos of model interpretability: In machine learning, the concept of interpretability is both important and slippery. *Queue*, 16(3):31–57, 2018.
- Zhou Lu, Hongming Pu, Feicheng Wang, Zhiqiang Hu, and Liwei Wang. The expressive power of neural networks: a view from the width. In *Proceedings of the 31st International Conference on Neural Information Processing Systems*, page 6232–6240, 2017. ISBN 9781510860964.
- A. G. Matthews, J. Hron, M. Rowland, R.E. Turner, and Z. Ghahramani. Gaussian process behaviour in wide deep neural networks. *ICLR*, 2018.
- R.M. Neal. Bayesian learning for neural networks. *Springer Science & Business Media*, 118, 1995.

- Anh Nguyen, Jason Yosinski, and Jeff Clune. Deep neural networks are easily fooled: High confidence predictions for unrecognizable images. In *Proceedings of the IEEE conference on computer vision and pattern recognition*, pages 427–436, 2015.
- Oscar Oelrich, Shutong Ding, Måns Magnusson, Aki Vehtari, and Mattias Villani. When are bayesian model probabilities overconfident?, 2020.
- Ilsang Ohn and Lizhen Lin. Adaptive variational bayes: Optimality, computation and applications. *The Annals of Statistics*, 52(1):335–363, 2024.
- Yaniv Ovadia, Emily Fertig, Jie Ren, Zachary Nado, D. Sculley, Sebastian Nowozin, Joshua Dillon, Balaji Lakshminarayanan, and Jasper Snoek. Can you trust your model's uncertainty? evaluating predictive uncertainty under dataset shift. In *Advances in Neural Information Processing Systems*, volume 32, 2019.
- T. Papamarkou, J. Hinkle, M. T. Young, and D. Womble. Challenges in Markov chain Monte Carlo for Bayesian neural networks. *Statistical Science*, 37(3):425–442, 2022.
- Du Phan, Neeraj Pradhan, and Martin Jankowiak. Composable effects for flexible and accelerated probabilistic programming in numpyro. In *Program Transformations for ML Workshop at NeurIPS*, 2019.
- Nicholas G Polson and Veronika Ročková. Posterior concentration for sparse deep learning. *Advances in Neural Information Processing Systems*, 31, 2018.
- Stuart Rogers, Michael Aftosmis, Shishir Pandya, Neal Chaderjian, Edward Tejnli, and Jasim Ahmad. Automated cfd parameter studies on distributed parallel computers. In *16th AIAA Computational Fluid Dynamics Conference*, page 4229, 2003.
- Donald B Rubin. The bayesian bootstrap. *The annals of statistics*, pages 130–134, 1981.
- David J Spiegelhalter, Nicola G Best, Bradley P Carlin, and Angelika Van Der Linde. Bayesian measures of model complexity and fit. *Journal of the royal statistical society: Series b (statistical methodology)*, 64(4):583–639, 2002.
- Christian Szegedy, Wojciech Zaremba, Ilya Sutskever, Joan Bruna, Dumitru Erhan, Ian Goodfellow, and Rob Fergus. Intriguing properties of neural networks. In *2nd International Conference on Learning Representations, ICLR 2014*, 2014.
- Hugo Touvron, Thibaut Lavril, Gautier Izacard, Xavier Martinet, Marie-Anne Lachaux, Timothée Lacroix, Baptiste Rozière, Naman Goyal, Eric Hambro, Faisal Azhar, Aurelien Rodriguez, Armand Joulin, Edouard Grave, and Guillaume Lample. Llama: Open and efficient foundation language models, 2023.
- Brian Trippe and Richard Turner. Overpruning in variational bayesian neural networks, 2018.
- Aki Vehtari and Janne Ojanen. A survey of bayesian predictive methods for model assessment, selection and comparison. *Statistics Surveys*, 6:142 – 228, 2012. doi: 10.1214/12-SS102.
- Aki Vehtari, Andrew Gelman, and Jonah Gabry. Practical bayesian model evaluation using leave-one-out cross-validation and waic. *Statistics and Computing*, 27(5):1413–1432, August 2016. ISSN 1573-1375.

- Aki Vehtari, Jonah Gabry, Måns Magnusson, Yuling Yao, and Andrew Gelman. Efficient leave-one-out cross-validation and waic for bayesian models, 2019. URL <https://mc-stan.org/loo>.
- Sumio Watanabe. Asymptotic equivalence of bayes cross validation and widely applicable information criterion in singular learning theory. *Journal of Machine Learning Research*, 11(116):3571–3594, 2010.
- Andrew G Wilson and Pavel Izmailov. Bayesian deep learning and a probabilistic perspective of generalization. *Advances in Neural Information Processing Systems*, 33:4697–4708, 2020.
- David H. Wolpert. The lack of a priori distinctions between learning algorithms. *Neural Computation*, 8(7):1341–1390, 10 1996. ISSN 0899-7667.
- Luhuan Wu and Sinead A Williamson. Posterior uncertainty quantification in neural networks using data augmentation. In *Proceedings of The 27th International Conference on Artificial Intelligence and Statistics*, volume 238 of *Proceedings of Machine Learning Research*, pages 3376–3384. PMLR, 02–04 May 2024.
- Yuling Yao, Aki Vehtari, Daniel Simpson, and Andrew Gelman. Using stacking to average bayesian predictive distributions (with discussion). *Bayesian Analysis*, 13(3), September 2018. ISSN 1936-0975. doi: 10.1214/17-ba1091.
- Yuling Yao, Aki Vehtari, and Andrew Gelman. Stacking for non-mixing bayesian computations: The curse and blessing of multimodal posteriors. *The Journal of Machine Learning Research*, 23(1):3426–3471, 2022.
- Chiyuan Zhang, Samy Bengio, Moritz Hardt, Benjamin Recht, and Oriol Vinyals. Understanding deep learning (still) requires rethinking generalization. *Communications of the ACM*, 64(3):107–115, 2021.

A Metrics and Practicalities

Recall that we denoted the training data to be $\mathcal{D} = \{x_n, y_n\}_{i=1}^N$ and the new data for testing to be $\tilde{\mathcal{D}} = \{\tilde{x}_n, \tilde{y}_n\}_{n=1}^{\tilde{N}}$. Denote the approximated posterior predictive mean as \mathbf{y} , the set of S samples of the signal as $\boldsymbol{\mu}^S$ and of the observations as \mathbf{y}^S . Upon computing the posterior predictive distribution, we obtain the root mean squared error and the empirical coverage as:

$$\text{RMSE} = \sqrt{\frac{1}{N} \sum_n^N [(\tilde{y}_n - \mathbb{E}^S[y_i^S])^2]},$$

$$\text{EC} = \frac{\#\{\mathbf{y} \in [q_{0.025}, q_{0.975}]\}}{N}, \text{ where } q \text{ are quantiles of } \boldsymbol{\mu}^S \text{ or } \mathbf{y}^S.$$

The results are obtained when the number of iterations of mfVI is set 10^4 , 10^4 , 5×10^4 , 6×10^4 to train models with, respectively, 20, 200, 1000, 2000 hidden units in a layer. In models trained with HMC, the number of samples used for warmup was set to 10^3 , the samples used for posterior is 10^3 in models with 20 hidden units, and 2×10^3 in models with 200, 1000, 2000 hidden units in a layer. Across all the experiments with simulated data, the

learning rate of the optimizer is set to $5e - 3$. In deeper networks, the number of iterations of mfVI was set to $L \times 10^4$; the HMC had the number of warmup samples fixed to 10^3 and the number of samples was $\min(4 \times 10^3, L \times 10^3)$.

When evaluating BNN's performance on the NASA's rocket booster simulation, we only considered mfVI, and set the number of iterations to 10^4 and learning rate to $5e - 2$, with one exception of the OOD scenario and 200 hidden units, when we trained the model for 2×10^4 iterations.

Remark on the initialization. Based on the empirical evidence, we observed that in our experiment for $L = 1, 2$ the NumPyro implementation of mfVI requires the initialization mode to be set to "init to feasible", which chooses the initialization point uniformly (ignoring the prior distribution). Whereas for $L = 3, 4, 5, 6$ mfVI requires "init to mean", which sets initial parameters to the prior mean, and "init to feasible" will fail. Conversely, the NumPyro implementation of the HMC fails if the initialization location is set to "init to mean" but performs fine if it is always set to "init to feasible", i.e. ignoring the distribution parameters.

B Supplementary to Predictive Model Assessment

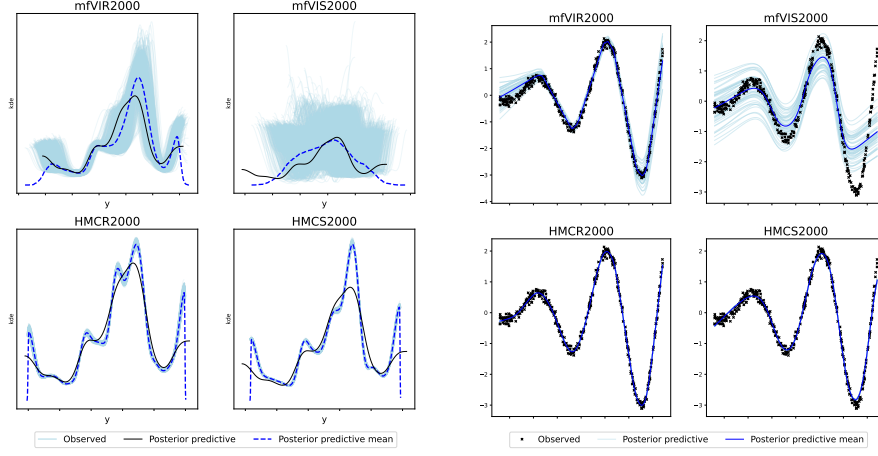
B.1 Empirical model assessment

Recall, the OOD scenario, where we have specifically created an extreme case when the training data \mathcal{D}_c and the new data $\tilde{\mathcal{D}}_c$ were covering disjoint regions of the true function. To assess the expected out-of-sample predictive performance, we could begin with posterior predictive checks (PPC), which compare the true \mathcal{D}_c to datasets simulated from the posterior predictive distribution [Gelman et al., 2020]. Figure 8a and Figure 9a provide the PPC based on the kernel density estimates of the observed \mathbf{y} , and Figure 8b and Figure 9b compare posterior predictive to the observed \mathbf{y} for all of the models with $D_1 = 2000$; both figures evidently classify the mean-field VI with sigmoid activation as inappropriate. However, it is not apparent that HMCS2000 is significantly inferior to HMCR2000. We compare the RMSE computed in the OOD settings to $\widehat{\text{elpd}}_{\text{loo}}$ estimates. Since the idea of estimating the expected log predictive density is in evaluating future predictive performance, we expect the higher $\widehat{\text{elpd}}_{\text{loo}}$ to correspond to a better model and lower RMSE. Indeed, Figure 8c and Figure 9c are more informative in this sense than PPC diagnostics, and we observe the inverse dependence between $\widehat{\text{elpd}}_{\text{loo}}$ and RMSE. Sampling and approximation techniques result in different scales of $\widehat{\text{elpd}}_{\text{loo}}$ estimates (in general, $\widehat{\text{elpd}}_{\text{loo}}$ is lower for VI, especially, in wide networks) and thus, we compare the models trained with different algorithms for better visualization.

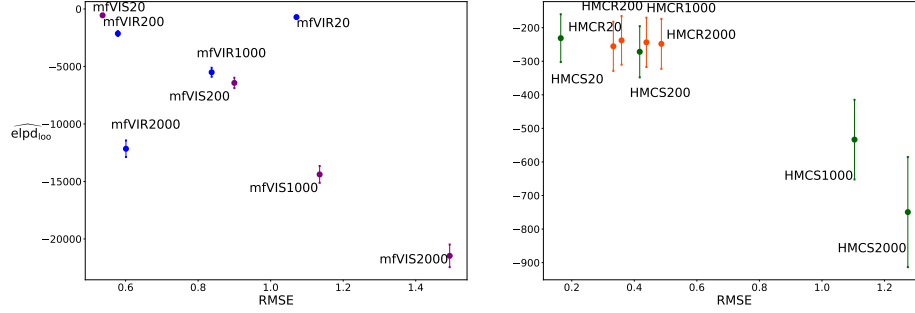
General summary. In certain cases, such as mfVIS for large width, the posterior predictive checks are able to detect an undesirable model. However, when the PPCs are not sufficient, we confirmed that the PSIS-LOO estimates of the expected log pointwise predictive density can serve as robust diagnostics for both the mfVI and the HMC methods.

B.2 Correspondence Between WAIC and RMSE

Above, we compared the RMSE obtained in the OOD experiment to the estimates of the expected log pointwise predictive density obtained with LOO-CV. An alternative approach is to overestimate the elpd by first computing the log pointwise predictive density of \mathcal{D} and then adjusting it by some correction term. Specifically, suppose that $\boldsymbol{\theta}$ are the parameters of the model and $\boldsymbol{\theta}^s, s = 1, \dots, S$ are simulation draws. Then, one can evaluate the log



(a) Posterior predictive checks for the (b) Posterior predictive distribution and wider models based on the kernel density posterior predictive mean compared to estimates of the observed y .



(c) The correspondence between the $\widehat{\text{elpd}}_{100}$ and the RMSE in the OOD scenario. Higher $\widehat{\text{elpd}}_{100}$ should correspond to lower RMSE.

Figure 8: Estimating the out-of-distribution performance of models with Gaussian priors before seeing the new data: testing the (a), (b) PPC and (c) $\widehat{\text{elpd}}_{100}$. The mfVIR2000 is confirmed to be unreliable in all methods. The PPC of the HMCS2000 does not provide enough information to judge its performance in the OOD settings, while the $\widehat{\text{elpd}}_{100}$ does.

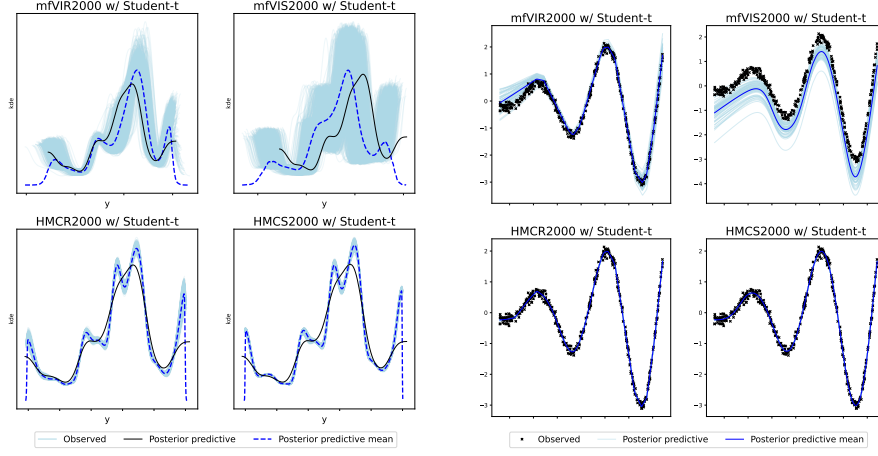
pointwise predictive density as

$$\widehat{\text{lpd}} = \sum_{n=1}^N \log \left[\frac{1}{S} \sum_{s=1}^S p(y_n | \theta^s) \right].$$

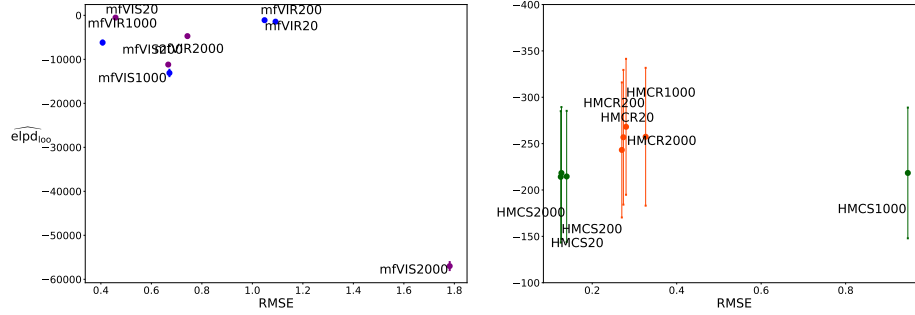
With $\widehat{\text{lpd}}$ at hand, a superior successor of the Akaike Information criterion (AIC) [Akaike, 1998] and the Deviance information criterion (DIC) [Spiegelhalter et al., 2002] called the Watanabe-Akaike information criterion (WAIC)² [Watanabe, 2010] can be obtained. To mitigate the bias between the log pointwise density and the expected utility, WAIC subtracts the simulation-estimated effective number of parameters:

$$\widehat{\text{elpd}}_{\text{WAIC}} = \widehat{\text{lpd}} - \widehat{p}_{\text{WAIC}}, \text{ where } \widehat{p}_{\text{WAIC}} = \sum_{n=1}^N \text{Var}^S(p(y_n | \theta^s)).$$

²Also called Widely Applicable information criterion



(a) Posterior predictive checks for the (b) Posterior predictive distribution and wider models based on the kernel density posterior predictive mean compared to estimates of the observed y .



(c) The correspondence between the $\widehat{\text{elpd}}_{\text{loo}}$ and the RMSE in the OOD scenario. Higher $\widehat{\text{elpd}}_{\text{loo}}$ should correspond to lower RMSE.

Figure 9: Estimating the out-of-distribution performance of models with Student-t priors before seeing the new data: testing the (a), (b) PPC and (c) $\widehat{\text{elpd}}_{\text{loo}}$. The mfVIR2000 is confirmed to be unreliable in all methods. The PPC of the HMCS2000 does not provide enough information to judge its performance in the OOD settings, while the $\widehat{\text{elpd}}_{\text{loo}}$ does.

Here, Var^S is the sample variance and the estimated effective number of parameters \hat{p}_{WAIC} can be seen as a measure of model complexity. Asymptotically, WAIC is equivalent to the Bayesian leave-one-out cross-validation (LOO-CV) estimate of the expected utility [Watanabe, 2010]. Even though cross-validation is a natural framework for accessing the model's predictive performance, the WAIC was for a long time preferred over the LOO-CV due to the computational challenges arising from multiple model runs [Gelman et al., 2014]. Moreover, whilst both the PSIS-LOO and WAIC estimates give nearly unbiased estimates of the predictive ability of the model, $\widehat{\text{elpd}}_{\text{loo}}$ was shown to be more robust than $\widehat{\text{elpd}}_{\text{WAIC}}$; in the presence of limited sample size and weak priors, WAIC can severely underestimate \hat{p}_{WAIC} and often has a larger bias towards the log predictive density [Vehtari et al., 2016, Gelman et al., 2014].

That said, computing $\widehat{\text{elpd}}_{\text{loo}}$ involved Pareto smoothed importance sampling, and in some of the models, the estimated shape parameter of the generalized Pareto distribution gave a warning about the reliability of the LOO estimate. Here, we do an extra step and

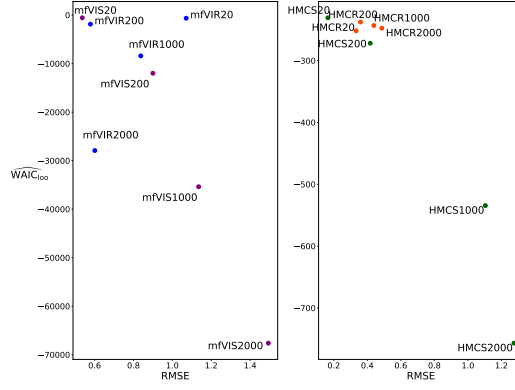


Figure 10: Estimating the out-of-distribution performance before seeing the new data: the correspondence between the $\widehat{\text{elpd}}_{\text{WAIC}}$ and the RMSE in the OOD scenario. Similarly to $\widehat{\text{elpd}}_{100}$, the higher $\widehat{\text{elpd}}_{\text{WAIC}}$ should correspond to lower RMSE.

check if the WAIC and LOO estimates of the elpd agree in the case of models with Gaussian priors. Figure 10 illustrates the reverse dependency between the RMSE and $\widehat{\text{elpd}}_{\text{WAIC}}$ and is largely identical to the figure illustrating the dependency between the RMSE and $\widehat{\text{elpd}}_{100}$ (in terms of the location of coordinates but not the error bars). Therefore, we can conclude that LOO estimates of the elphd can be seen as relatively reliable.

C Supplementary for Student-t Priors

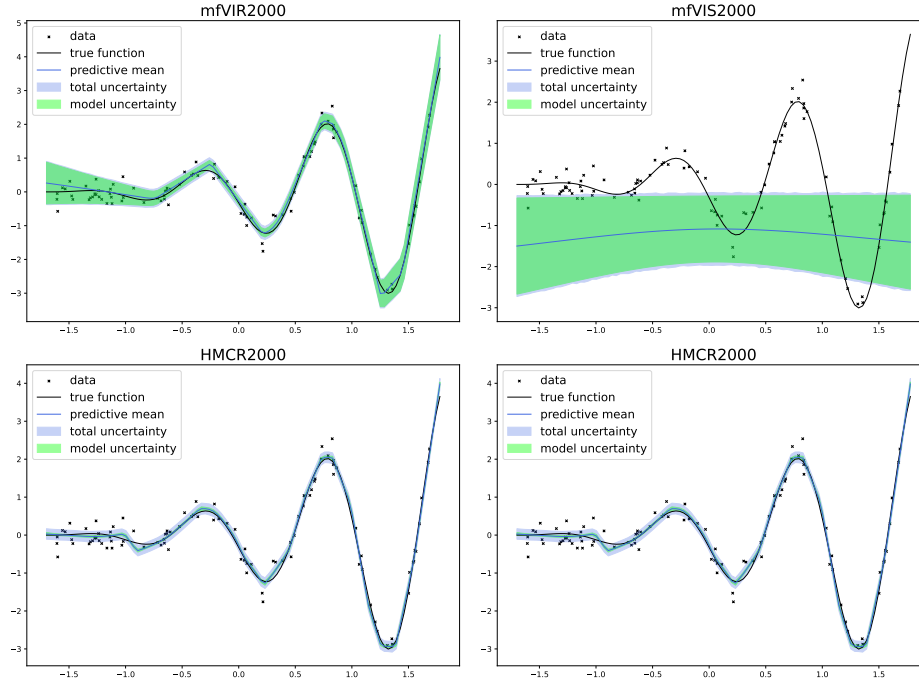


Figure 11: The predictions and uncertainty estimates obtained by each model for $D_1 = 2000$ and Student-t priors.

In the main body of the work, we first studied the performances of mfVIR, mfVIS, HMCR and HMCS with 1 hidden layer and either Gaussian or Student-t priors as the width increases. The predictions of all four models with Student-t priors when $D_1 = 2000$ are provided on the Figure 11. Similar to models with Gaussian priors, the performance of the mfVIS dips with the increase in the dimension of the hidden layer; for wider networks, its posterior predictive distribution fails to capture the data, and degenerates to the prior. The HMCR2000 model exhibits a better performance than the HMCS2000 both in terms of accuracy and uncertainty quantification.

Consider BNNs with Student-t priors with the number of layers L varying from 1 to 6 and a fixed number of hidden units in each layer $D_h = 20$, then Figure 12 illustrates the predictions of all four models with $L = 6$

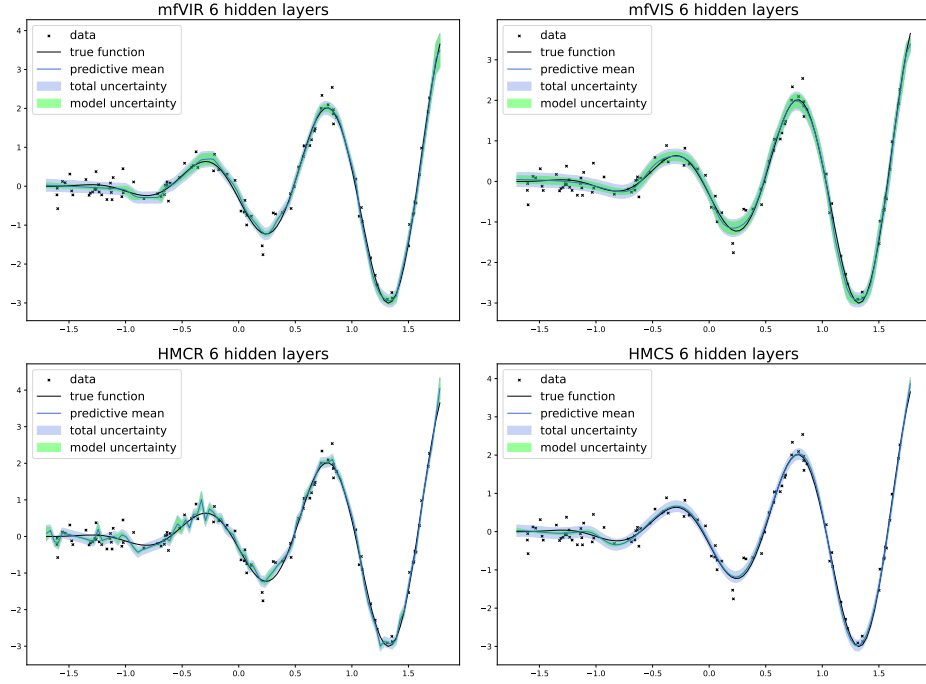


Figure 12: The predictions and uncertainty estimates obtained by each model for $L = 6$ and Student-t priors.

Further, Figure 13 compares non-OOD and OOD predictions obtained by the BNNs with ReLU activation, Student-t priors and $D_1 = 200$.

D Supplementary to Ensembles and Averages

Remark on constructing deep ensembles. Given $\mathcal{M} = \{M_1, \dots, M_K\}$ a collection of models suppose that K approximations $\tilde{\mathbf{y}}_k$ of the posterior $p(\tilde{\mathbf{y}}|\mathcal{D}, M_k)$ have means μ_k and variances σ_k^2 or $k = 1, \dots, K$. Then the mean and variance of an ensemble of approximations:

$$\mu_{\text{DE}} = K^{-1} \sum_1^K \mu_k, \quad \sigma_{\text{DE}}^2 = K^{-1} \sum_1^K \sigma_k^2 + \mu_k^2 - \mu_{\text{DE}}^2.$$

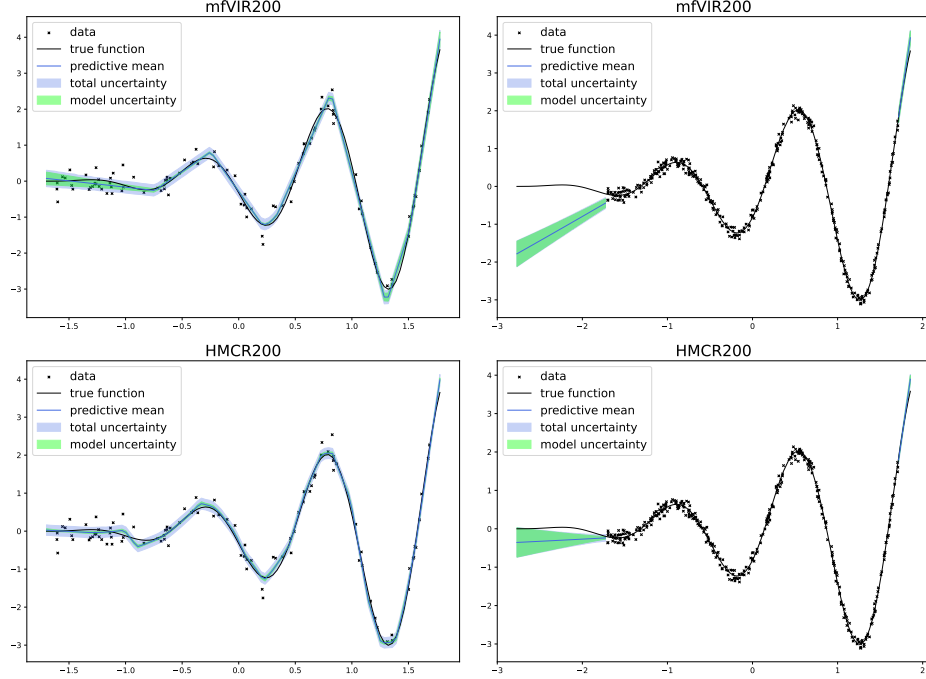


Figure 13: Within-the sample and out-of-sample predictions and uncertainty estimates of BNNs with $D_1 = 200$, ReLU activation and Student-t priors.

In general, given weights $\omega_k = p(M = M_k)$ the mean and the variance are

$$\begin{aligned}\mu_{\text{DE}} &= \mathbb{E}[\mathbb{E}[\tilde{\mathbf{y}}|M]] = \sum_1^K \omega_k \mu_k, \\ \sigma_{\text{DE}}^2 &= \mathbb{E}[\mathbb{E}[\tilde{\mathbf{y}}^2|M]] - \mu_{\text{DE}}^2 = \sum_1^K \omega_k \mathbb{E}[\tilde{\mathbf{y}}_k^2] - \mu_{\text{DE}}^2 \\ &= \sum_1^K \omega_k (\sigma_k^2 + \mu_k^2) - \mu_{\text{DE}}^2.\end{aligned}$$

D.1 Models with Student-t priors

Consider the mfVIR20 model with Student-t priors, the 'complement-distributions' and the 'related-distributions' OOD tasks. In each task, we obtain 10 posterior predictive distributions and construct ensemble, pseudo-BMA and stacking approximations, the results are illustrated Figure 14.

D.2 Deeper Networks

Based on the 10 posterior predictive distributions obtained starting from 10 different random initialization points, we construct ensemble, pseudo-BMA and stacking approximations for mfVIR and mfVIS models with Gaussian priors and $L = 6$ hidden layers. The results are consistent with the observation made in the main body of the work; in the 'complement-distributions' task (Figure 15) pseudo-BMA is confirmed to be inferior to stacking and deep

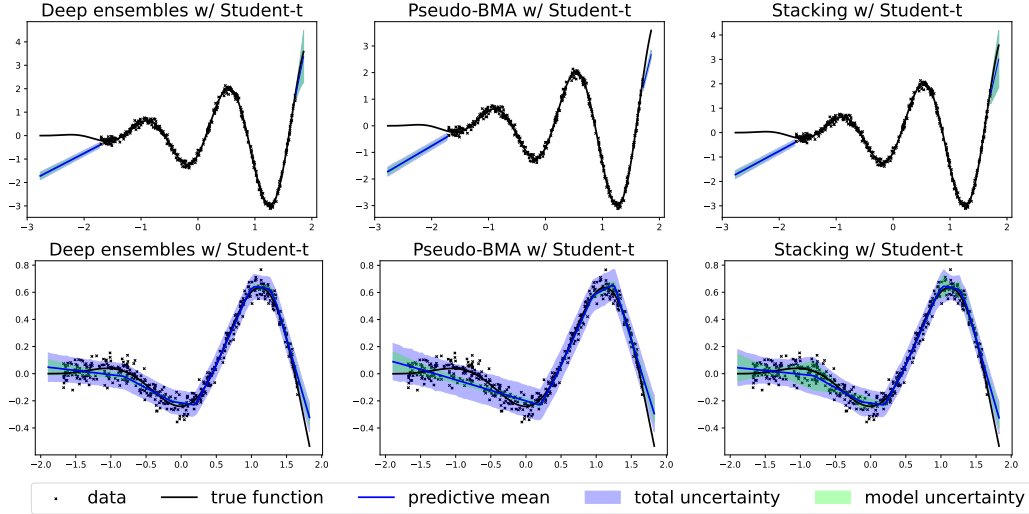


Figure 14: Predictions obtained by ensembling, stacking and pseudo-BMA when applied to mfVIR20 with Student-t priors in the 'complement-distributions' (top) and 'related-distributions' (bottom) OOD tasks. The pseudo-BMA is worse than DE and stacking, which are very similar to each other.

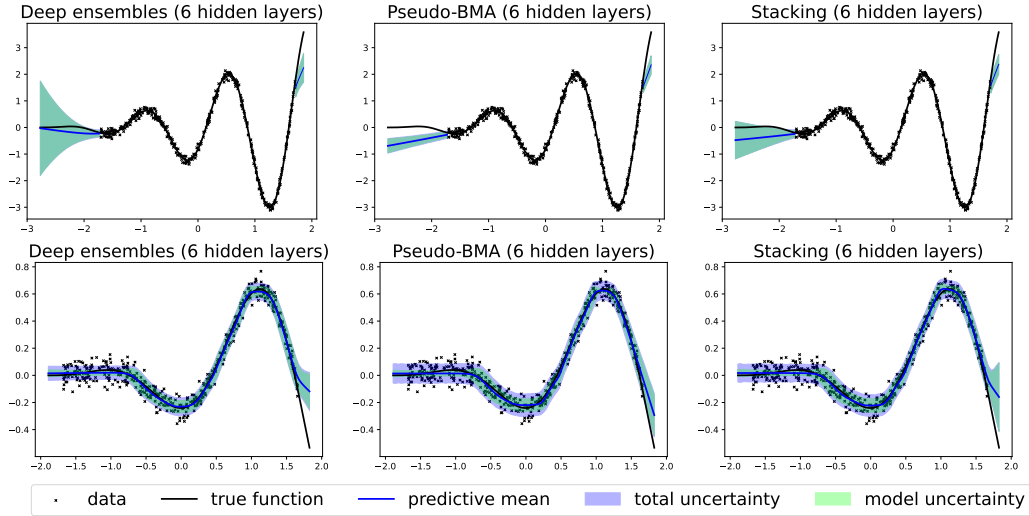


Figure 15: Predictions obtained by ensembling, stacking and pseudo-BMA when applied to mfVIR20 with $L = 6$ in the 'complement-distributions' (top) and the 'related-distributions' (bottom) task.

ensembles of BNNs. In the related distribution task (Figure 15), in terms of both accuracy and uncertainty quantification, stacking is preferable over deep ensembles and pseudo-BMA with the latter performing better than ensembles (unlike in the one-layer case).

D.3 Supplementary to the Rocket Booster Simulation

When considering the Langley Glide-Back Booster simulator data [Rogers et al., 2003], we evaluated the performance of the mfVIR for various widths and in both non-OOD and

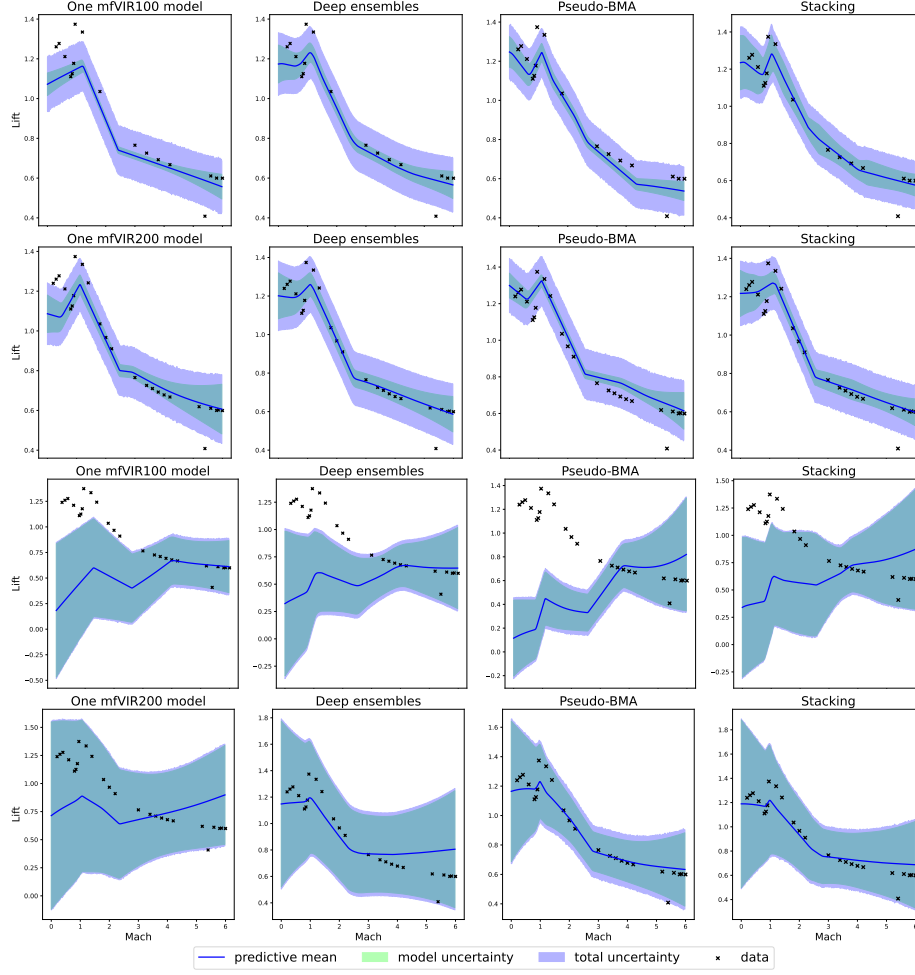


Figure 16: Slices of predicted lift obtained by a single model and by ensembling, stacking and pseudo-BMA when applied to mfVIR100 and mfVIR200 with Gaussian priors in the non-OOD (top figures) and 'complement-distributions' OOD (bottom figures) tasks. Stacking outperforms other methodologies.

'complement-distributions' tasks. Here we provide additional figures for models with 100 and 200 hidden units illustrating the slices of predicting lift, with Mach on the x-axis and angles α and β fixed to 25 and 4, respectively.